Dispersed laser-induced fluorescence of molecular ions. Identification of new low-lying electronic states of TiCl+ and TiF+

ARTICLE *in* CHEMICAL PHYSICS · SEPTEMBER 1999

Impact Factor: 1.65 · DOI: 10.1016/S0301-0104(99)00215-3

2 AUTHORS, INCLUDING:

Cristian Focsa
Université des Sciences et Technologi…

101 PUBLICATIONS **941** CITATIONS

ELSEVIER

Chemical Physics 247 (1999) 395–405

Chemical Physics

www.elsevier.nl/locate/chemphys

Dispersed laser-induced fluorescence of molecular ions. Identification of new low-lying electronic states of $TiCl^+$ and TiF^+

C. Focsa [1], B. Pinchemel *

Laboratoire de Physique des Lasers, Atomes et Molécules, UMR CNRS 8523, Centre d'Etudes et de Recherches Lasers et Applications, Bât. P5, Université des Sciences et Technologies de Lille, 59655 Villeneuve d'Ascq cedex, France

Received 24 March 1999

Abstract

The dispersed laser-induced fluorescence technique has been applied for the first time to metallic molecular ions. The $TiCl^+$ and TiF^+ ions were produced by a high-voltage discharge in helium with traces of $TiCl_4$ or TiF_4. A c.w. dye-laser and a grating plate spectrometer were used to record low-resolution spectra of these species in the visible. This leads to the observation of new low-lying electronic states of these ions: the $C^3\Pi$ (~ 1535 cm^{-1}) state of $TiCl^+$, the $B^3\Delta$ (~ 2040 cm^{-1}) and $C^3\Pi$ (~ 2200 cm^{-1}) states of TiF^+. The identification of these new states contributes to a better characterisation of the first 3000 cm^{-1} of the energy level diagrams of these molecules. The experimental position of the $C^3\Pi$ state of $TiCl^+$ is in good agreement with theoretical predictions given by a Ligand Field Theory model [C. Focsa, M. Bencheikh, L.G.M. Pettersson, J. Phys. B: At. Mol. Opt. Phys. 31 (1998) 2857]. We have extended these calculations to the TiF^+ isovalent ion, taking advantage of the new experimental data. Both experimental and theoretical new results presented in this paper are expected to help future investigations on these species.

1. Introduction

In the recent past, several papers have been devoted to spectroscopic studies of $TiCl^+$ [1–4] and TiF^+ [5] ions. Laser techniques such as velocity modulation [6] or concentration modulation [7] allowed to record high resolution spectra leading to the identification of electronic states through the rotational analysis of bands observed in the yellow–green spectral region. At the same time, theoretical works [4,8,9], using a Ligand Field model, were performed in order to determine the relative positions and the nature of the low-lying states of $TiCl^+$.

The quoted experimental techniques are based on absorption of the laser light by the ions. As a consequence, only the ground state and possibly electronic states lying in the first 1000 cm^{-1} above the ground state are found to be populated enough in order to allow the ions to be excited in an upper electronic state by the laser light. For example, using velocity modulation laser spectroscopy, it has been possible

* Corresponding author. Tel.: +33-3-20-43-49-81; fax: +33-3-20-43-40-84; E-mail: bernard.pinchemel@univ-lille1.fr

[1] Present address: Department of Chemistry, University of Waterloo, Waterloo, Ontario, Canada N2L 3G1.

0301-0104/99/$ - see front matter
PII: S0301-0104(99)00215-3

to identify the $A^3\Delta$ state of $TiCl^+$ (thanks to the $[17.8]^3\Delta - A^3\Delta$ transition) located at about 350 cm^{-1} above the $X^3\Phi$ ground state when the $C^3\Pi$ state, theoretically located [8] at more than 1500 cm^{-1} above the ground state has not been evidenced.

Historically, emission spectra recorded from a hollow cathode discharge allowed the first observation of the most intense electronic transitions of the $TiCl^+$ ion [10] in the yellow–green spectral region, but the signal was very weak and no trace of the $[17.8]^3\Delta - A^3\Delta$ transition nor of any satellite bands have been detected then. Moreover, emission spectroscopy, on the contrary of laser modulation techniques, does not allow to record spectra of ionic species free of signal arising from neutral compounds simultaneously produced in the discharge. Nevertheless it turns out that these techniques must be considered as complementary. The study of TiF^+ is an example: in a first time we recorded a low resolution spectrum from the light emitted by the positive column of the high-voltage source used for laser modulation velocity experiments: the observation of three blue shaded groups of Q and P heads suggested the presence of a triplet–triplet transition which revealed to be the $[17.6]^3\Delta - X^3\Phi$ transition of TiF^+ when studied at high resolution by the velocity modulation laser technique [5]. This coarse observation allowed to start laser scans at less than 1 cm^{-1} from band-heads preventing time-consuming sampling of large spectral regions. Both for $TiCl^+$ and TiF^+, no evidence of transitions other than those studied in Refs. [1–5,10] were observed neither in velocity modulation laser experiments nor in emission spectra.

It was then tempting to see if dispersed laser-induced fluorescence could be a way to detect new band systems. It is well known that concentration of ions in electric discharges is several orders of magnitude smaller compared to neutral molecules concentration. In contrast with long pass absorption techniques which overcome this difficulty, a fluorescence signal takes place in a small area of the discharge, generally no larger than the entrance slit of the spectrometer. All the studies devoted up to now to laser-induced fluorescence of ions were performed by fast-ion-beam spectroscopy, in a first time on atoms [11,12] and later on light diatomic (N_2^+ [13]) and triatomic (CO_2^+ [14,15]) molecules. This technique produces sufficiently intense beams of ions and gives access to high resolution spectra but it requires highly sophisticated equipment. In this paper we use a most conventional technique which is applied to metallic molecules which cannot be easily produced at very low pressure such as it is necessary for fast-ion-beam laser spectroscopy. Our purpose was to observe, at low resolution, transitions involving new electronic states.

$TiCl^+$ was a good candidate because this ion is relatively easy to produce. It is a 3d-transition-metal containing species for which several low-lying electronic states are expected to take place in the first 3000 cm^{-1} above the ground state as stated by theoretical calculations [4,8,9]. In addition the $[17.8]^3\Delta$ state is well known, especially its spin-orbit parameter is perfectly determined [1,2]. In all the present experiments this state will be used as upper state of the transitions looked for through their fluorescence signal.

This work has been performed at low resolution due to the weakness of the fluorescence signal, as a consequence no rotational structure has been fully resolved. Under these conditions, we observed the $[17.8]^3\Delta - C^3\Pi$ transition of $TiCl^+$. The same experimental set-up, adapted to the production of TiF^+, allowed the identification of two new $B^3\Delta$ and $C^3\Pi$ electronic states of this species through the observation of the $[17.6]^3\Delta - B^3\Delta$ and $[17.6]^3\Delta - C^3\Pi$ transitions. In addition some vibrational bands belonging to already known low-lying electronic states of $TiCl^+$ and TiF^+ have been identified.

These new experimental data collected on TiF^+ gave us the opportunity to perform Ligand Field Theory (LFT) calculations on this species using the same model already employed for the study of the $TiCl^+$ isovalent ion [8].

2. Experiment

A glass cell with six orthogonal apertures has been used. At the extremities of the 25 cm-long horizontal arms (1 cm inner diameter) are located stainless steel electrodes. In the central perpendicular plane is the horizontal gas inlet facing the observation window and the two vertical apertures allowing the laser beam to enter the cell parallel to the entrance slit of the spectrometer.

Ions are produced by an electric discharge in helium with traces of $TiCl_4$ (or TiF_4) at a total pressure of 10 Torr. The ac discharge (4 kV peak to peak, $I = 400$ mA), driven at 30 kHz, ensures a more stable signal than when a dc discharge is used. The cell is exhausted by a two stages mechanic pump through two exits located close to the electrodes.

The laser beam is produced by a c.w. Coherent dye laser in a linear configuration to provide a 1 cm^{-1} broadband line in order to populate simultaneously several rotational levels. Rhodamine 110 dye, pumped by 8 W of an Ar^+ laser, delivered 1.5 W at 560 nm. The fluorescence signal is dispersed through a 1.5 m focal length Jobin–Yvon spectrometer, the entrance slit of which is 50 to 200 μm large depending on the intensity of the fluorescence signal. The dispersed light is collected on a Hamamatsu C.C.D. detector (20 mm × 3 mm) which covers a 3 nm-large spectral region in the single-pass configuration of the spectrometer. The weak fluoresce signal is overflowed by the intense light emission of the positive column of the discharge. Typically the fluorescence signal is only a few percent of the emission. The fluorescence signal has been extracted from the emission by subtracting each other two recordings of the same spectral range, the first with the laser on, the second in absence of laser excitation. This has been made possible thanks to the stability of the discharge. In a few cases, the atomic lines remained slightly visible when recordings lasted longer than 30 s. The numerous Ti atomic lines were used for calibration.

3. Observation of new bands of $TiCl^+$

The efficiency of the method has been first tested on the well known $[17.8]^3\Delta - X^3\Phi$ transition of $TiCl^+$ [1]. The first fluorescence signal has been observed in the Q branch of the $[17.8]^3\Delta_1 - X^3\Phi_2$ (0–0) band when the laser was tuned on the P head. The same kind of signal has been observed in the Q branches of the two other sub-bands of the $[17.8]^3\Delta - X^3\Phi$ (0–0) transition when the laser was tuned on their P heads. Intensities of the fluorescence of the three Q branches decrease roughly in the ratio 10:8:3 due to the increasing energy positions of the successively laser-pumped $X^3\Phi_2$ ($v = 0$, 0 cm^{-1}), $X^3\Phi_3$ ($v = 0$, 189 cm^{-1}) and $X^3\Phi_4$ ($v = 0$, 363 cm^{-1}) spin-orbit components of the ground state [1]. In each case weak fluorescence of the two other sub-bands was simultaneously observed. We note that the shape of these bands is comparable to that obtained from emission spectra. This suggests that transfers are induced between the spin-orbit components of the upper $[17.8]^3\Delta$ state by collisions of $TiCl^+$ ions with He atoms due to the high pressure (10 Torr) of the plasma, inducing a relaxation between the rotational levels.

All along this paper, unless quoted, the upper state of the studied transitions will be considered to be populated by the laser tuned on the P head of the most favourable $^3\Delta - X^3\Phi$ sub-band for this purpose. As an example, Fig. 1 displays the fluorescence of the $[17.8]^3\Delta_1 - A^3\Delta_1$ (0–0) sub-band, its intensity is good enough to partially resolve the rotational structure of the P branch when the en-

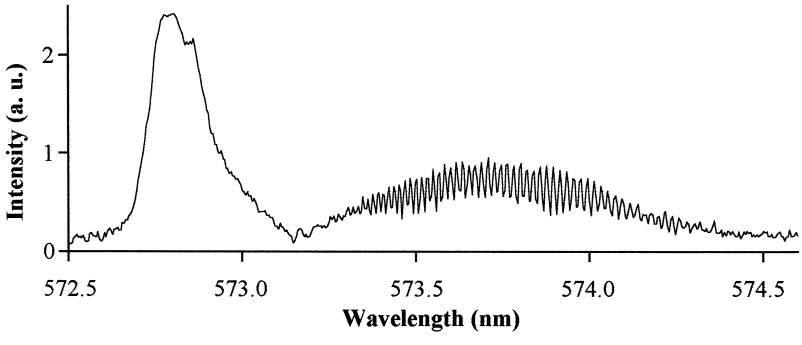

Fig. 1. Dispersed laser-induced fluorescence of the $[17.8]^3\Delta_1 - A^3\Delta_1$ (0–0) transition of $TiCl^+$. The laser line is tuned on the P head of the $[17.8]^3\Delta_1 - X^3\Phi_2$ (0–0) band at 559.6 nm.

Table 1
Positions (in cm^{-1}) of the estimated origins of the newly observed bands of $TiCl^+$ and TiF^+, experimental uncertainties are estimated to 2 cm^{-1}. The upper levels of the transitions refer to the $[17.8]^3\Delta$ ($TiCl^+$) or $[17.6]^3\Delta$ (TiF^+) states

Transition	$TiCl^+$	TiF^+
$^3\Delta_1 - {}^3\Delta_1(0–1)$	16966	
$^3\Delta_1$-unassigned level	16863	
$^3\Delta_1 - X^3\Phi_2(0–1)$		16857
$^3\Delta_1 - X^3\Phi_3(0–1)$		16908
$^3\Delta_1 - X^3\Phi_4(0–1)$		16966
$^3\Delta_2 - {}^3\Delta_2(0–0)$		15624
$^3\Delta_1 - {}^3\Delta_1(0–0)$		15606
$^3\Delta_3 - {}^3\Pi_2(0–0)$	16349[a]	
$^3\Delta_2 - {}^3\Pi_1(0–0)$	16247[a]	15461
$^3\Delta_1 - {}^3\Pi_0(0–0)$	16187[a]	15403
	16195	

[a] Head position.

trance slit of the spectrometer is 50 μm large. We note that about 60 rotational lines are simultaneously observed, this value is three times larger than the 20 lines covered by the 1 cm^{-1} wide laser line tuned on the P head of the $[17.8]^3\Delta_1 - X^3\Phi_2$ (0–0) band. This confirms the occurrence of rotational relaxation.

The next step has been to look for the $[17.8]^3\Delta - C^3\Pi$ transition of $TiCl^+$ that theoretical calculations [8] suggested to be found in the 605–615 nm spectral region. Tuning the laser line on the P head of each of the three sub-bands of the $[17.8]^3\Delta - X^3\Pi$ (0–0) transition, it has been possible to observe three band structures, the most intense head of which being located at 611.5 nm (identified as the $[17.8]^3\Delta_3 - C^3\Pi_2$ transition), 615.3 nm ($[17.8]^3\Delta_2 - C^3\Pi_1$) and 617.6 nm ($[17.8]^3\Delta_1 - C^3\Pi_0$). The structure of these bands is somewhat puzzling. This can be due to perturbations suspected to occur between the $C^3\Pi$ state and close-lying vibrational levels of the $A^3\Delta$ state. In addition the $B^3\Sigma^-$ state is expected to lie in the same spectral region [8] and could interact with the $C^3\Pi$ state. We can remind that strong perturbations, inducing satellite bands, occur between the $X^3\Phi$ ($v = 1$) and the $A^3\Delta$ ($v = 0$) states, mainly for the $\Omega = 2$ and $\Omega = 3$ spin components [2]. At this stage of the study, only high resolution spectroscopy could provide more detailed information about the band structure. Nevertheless, laser-induced fluorescence, on the difference of emission spectroscopy, gives useful information on the states involved in the observed transitions because the nature of the upper laser-populated electronic state is here well determined.

A systematic survey of the 560–610 nm spectral region has been done in order to search for new vibrational bands of the $[17.8]^3\Delta - X^3\Phi$ and $[17.8]^3\Delta - A^3\Delta$ transitions. A weak band without Q branch has been observed at 16966 cm^{-1}, the upper state of which is the $[17.8]^3\Delta_1$ ($v = 0$). The lower state takes place at 907 cm^{-1} in the energy level diagram, i.e. 476 cm^{-1} above the $A^3\Delta_1$ ($v = 0$) state. This value is close from $\Delta G_{1/2} = \omega_e'' - 2\omega_e'' x_e'' = 484$ cm^{-1} determined for the $X^3\Phi$ state from semi-empirical expressions [1]. This supports the assumption that the newly identified state is the $v = 1$ vibrational level of the $A^3\Delta_1$ state because the vibrational constants of these two close-lying states are expected to be very similar on the basis of the rotational analysis previously performed [2]. Under the same excitation conditions another weak transition with Q and P heads is observed at 16863 cm^{-1}. The lower state of this transition is located at 1010 cm^{-1} in the energy level diagram. It turns out that this state cannot be the $X^3\Phi_2$ ($v = 2$) state which is expected to lie at 952 cm^{-1} [4]. The hypothesis of a satellite band of the $[17.8]^3\Delta - A^3\Delta$ (0–1) transition cannot be securely suggested in absence of a rotational analysis. The experimental positions of the newly observed bands are summarised in Table 1. The derived positions of

Table 2
Excitation energies (in cm^{-1}) of the newly identified vibronic levels of $TiCl^+$ and TiF^+. E_2, E_3 and E_4 are respectively the energy of the $^3\Phi_2(v = 0)$, $^3\Phi_3(v = 0)$ and $^3\Phi_4(v = 0)$ spin-orbit components of the $X^3\Phi$ ground state of TiF^+

Vibronic level	$TiCl^+$	TiF^+
$^3\Pi_2(v = 0)$	1769	
$^3\Pi_1(v = 0)$	1729	$E_3 + 2202$
$^3\Pi_0(v = 0)$	1678	$E_2 + 2319$
$^3\Delta_2(v = 0)$		$E_3 + 2039$
$^3\Delta_1(v = 0)$		$E_2 + 2115$
Unassigned level	1010	
$^3\Delta_1(v = 1)$	907	
$^3\Phi_4(v = 1)$		$E_4 + 756$
$^3\Phi_3(v = 1)$		$E_3 + 755$
$^3\Phi_2(v = 1)$		$E_2 + 754$

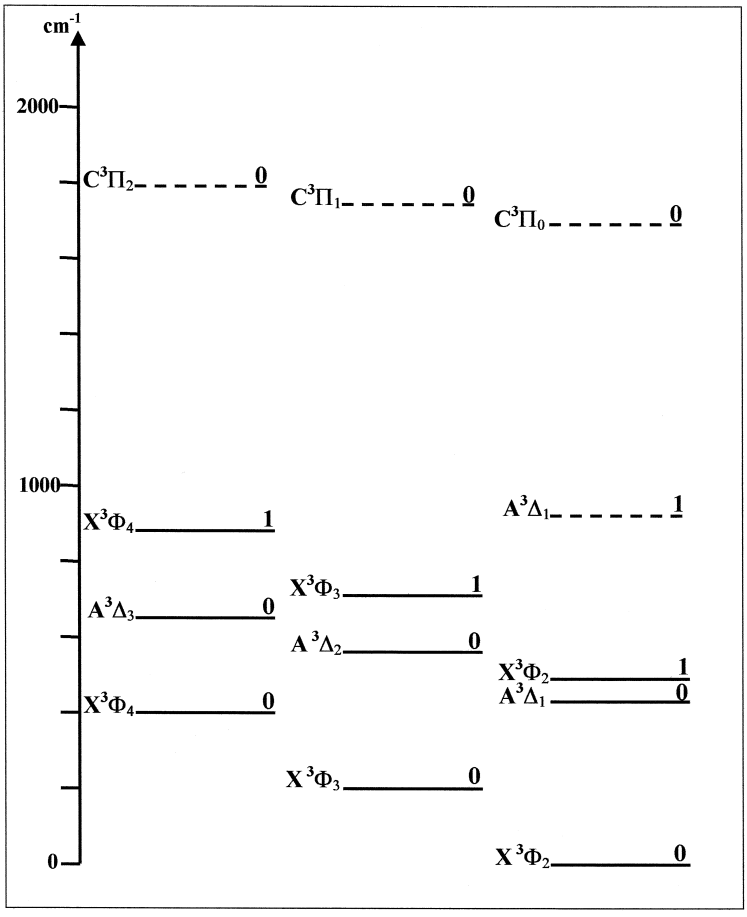

Fig. 2. Experimentally observed vibronic levels of the lowest electronic states of $TiCl^+$. The newly observed levels are in dashed lines.

the vibronic states are displayed in Table 2 and illustrated in Fig. 2.

4. Observation of new electronic states of TiF^+

In order to collect new spectral information about TiF^+, a systematic study of the region to the red side of the $[17.6]^3\Delta - X^3\Phi$ (0–0) transition (565 nm) has been performed. Velocity modulation laser experiments taught [5] that the absorption signal for TiF^+ is about one order of magnitude less intense than that observed for $TiCl^+$. In addition the experimental conditions are less easy to optimise: the vapour of TiF_4 is produced from heated TiF_4 powder, its flow is more difficult to adjust when compared to liquid $TiCl_4$ injected through a needle valve. It is not surprising that the recorded signals are weaker than in the case of $TiCl^+$. Let us remind now that in absence of satellite bands, it is not possible to fix the vibronic spin-orbit levels of TiF^+ in a common energy level diagram, i.e. the spin-orbit parameters of the electronic states are not experimentally determined, however they are theoretically estimated. The energies are then expressed as the distance from the $\Omega = 2$, 3 or 4 components of the $X^3\Phi$ ($v = 0$) state pumped by the laser.

A total of three groups of bands have been observed, in each case the laser has been successively tuned on the P head of the three spin-orbit sub-systems of the $[17.6]^3\Delta - X^3\Phi$ (0–0) transition.

The origins of the three bands of the first group are measured at 16 966 cm^{-1}, 16 908 cm^{-1} and 16 857 cm^{-1}, the lower levels of these transitions are respectively 756 cm^{-1}, 755 cm^{-1} and 754 cm^{-1} above the $\Omega = 2$, 3 and 4 spin-orbit components of the $X^3\Phi$ ($v = 0$) state. These values are in good agreement with the estimated values of $\Delta G_{1/2}(X^3\Phi) = 774$ cm^{-1} calculated from the values of $\omega_e(X^3\Phi) = 781$ cm^{-1} and $\omega_e x_e(X^3\Phi) = 3.4$ cm^{-1} derived from Kratzer and Pekeris expressions [16] for the $X^3\Phi$ state [5]. This suggests that the three lower states are the three spin-orbit components of the $X^3\Phi$ ($v = 1$) electronic ground state. The experimental values allow a direct calculation of $\omega_e(X^3\Phi) = 762$ cm^{-1} assuming that $\omega_e x_e(X^3\Phi)$ is kept equal to 3.4 cm^{-1}. A direct and more accurate determination of the ω_e parameter of the upper $[17.6]^3\Delta$ state can be then derived, it is equal to 860 cm^{-1} when it was previously estimated to 880 cm^{-1} assuming $\omega_e x_e([17.6]^3\Delta) = 3.8$ cm^{-1} from Pekeris relationship [5].

Scanning the spectral region toward the red, two close-lying weak bands have been discovered at 15 606 cm^{-1} and 15 624 cm^{-1} without evidence for a Q head. The third expected band has not been detected when the laser was tuned on the P head of the $[17.6]^3\Delta_3 - X^3\Phi_4$ (0–0) transition. The closeness of the two recorded bands suggests that the upper and lower states have almost the same spin-orbit splitting between their components. Let us assume that, as for corresponding states of $TiCl^+$ [1,2], the spin-orbit A parameters of the $X^3\Phi$, $B^3\Delta$, $C^3\Pi$ and $[17.6]^3\Delta$ states are similar. The splitting between two of the three spin-orbit sublevels of the electronic states is equal to A for a $^3\Pi$ state, 2A for a $^3\Delta$ state and 3A for a $^3\Phi$ state [16]. It turns out that the spin-orbit sub-bands arising from a $\Delta\Lambda = 0$ transition must be close lying and that the observed bands are most likely the $[17.6]^3\Delta_1 - B^3\Delta_1$ (0–0) transition at 15 624 cm^{-1} and the $[17.6]^3\Delta_2 - B^3\Delta_2$ (0–0) one at 15 606 cm^{-1}, the lower states of which are located at 2115 cm^{-1} and 2039 cm^{-1} above the $X^3\Phi_2$ ($v = 0$) and $X^3\Phi_3$ ($v = 0$) sublevels respectively (see Section 5 for the labelling of the $B^3\Delta$ state). Let us note that the $B^3\Delta$ state is located too high in energy above the $X^3\Phi$ state to be observed in velocity modulation experiments unlike the corresponding $A^3\Delta$ state of $TiCl^+$.

Two other bands have been recorded at 15 460 cm^{-1} and 15 402 cm^{-1} when the laser populates the $[17.6]^3\Delta_2$ and the $[17.6]^3\Delta_1$ sublevels, respectively. Both for TiF^+ and $TiCl^+$, the subsystems of the $^3\Delta - X^3\Phi$ transition take place in a decreasing energy order in the spectral range when the value of the quantum number Ω of the lower state goes from 2 to 4 [1,5]. The reason is that the splitting between the spin-orbit components is 1.5 times larger for the ground $X^3\Phi$ state than for the upper $^3\Delta$ state. The energy order of the two newly observed subsystems is the reversal of what is observed in the $[17.6]^3\Delta - X^3\Phi$ transition. As already observed for $TiCl^+$ in Section 3, this suggests that the lower levels of the

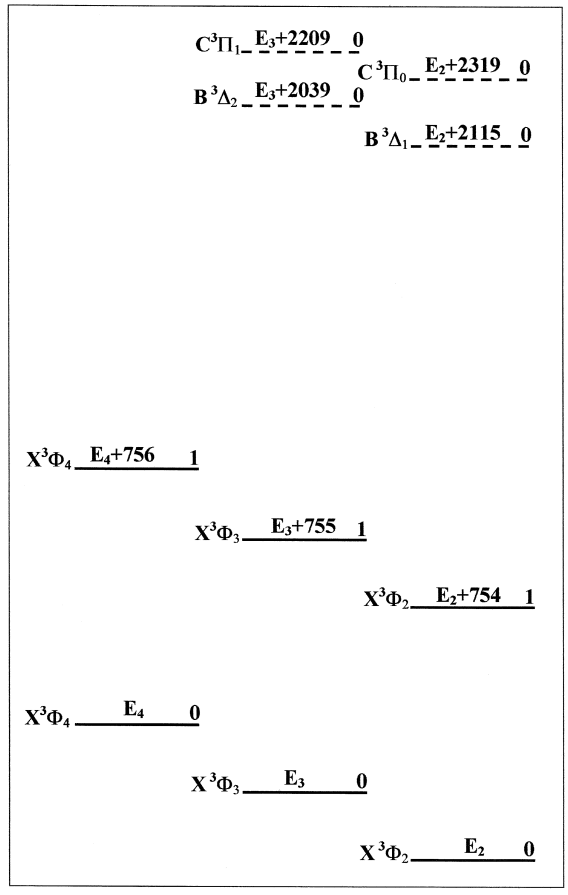

Fig. 3. Experimentally observed vibronic levels of the lowest electronic states of TiF^+. The newly observed levels are in dashed lines. In absence of satellite bands, the relative positions of the spin-orbit components are not determined.

transitions are the $\Omega = 0$ and 1 components of the $C^3\Pi$ state, taking place at 2202 cm^{-1} and 2319 cm^{-1} above the $X^3\Phi_3$ ($v = 0$) and $X^3\Phi_2$ ($v = 0$) sublevels of the ground state respectively. As already noted, no trace of the third spin-orbit subsystem of this transition has been detected. Experimental data concerning TiF^+ are summarised in Tables 1 and 2 to allow comparisons with results on $TiCl^+$. Fig. 3 displays the relative positions of the low-lying vibronic states of TiF^+.

5. Ligand field theory calculations on the electronic structure of TiF^+

Several theoretical works were published in the last years on the electronic structure of the $TiCl^+$ cation [4,8,9]. The LFT model used to describe this species was successively refined by using the new experimental findings from the groups of Lille [1,2] and Atlanta [3,4]. It is gratifying to note that the excitation energy (~ 1535 cm^{-1}) of the newly observed $C^3\Pi$ low-lying electronic state of $TiCl^+$ is in good agreement with our theoretically predicted value (~ 1400 cm^{-1}, see Table 5 of Ref. [8]).

The new experimental data that we report here for the TiF^+ ion give us the opportunity to extend the use of the LFT model employed for $TiCl^+$ to this isovalent species. The LFT treatment of TiF^+ can help to validate the Ti^{2+}–X^- (X = Cl, F) integer charge model and, on the other hand, can provide new predictions on the structure of the electronic spectrum of TiF^+. These predictions could be very helpful for future experimental observations.

The use of the Ti^{2+}–F^- ionic structure to describe the low-lying electronic states of TiF^+ is justified when considering the energetical criterion of Mandich et al. [17]. Roughly speaking, the lowest states of the $Ti^{2+}F^-$ and Ti^+F^0 structures are separated by:

$$\frac{2e^2}{R_e(TiF^+)} - [IP(TiII) - EA(F)] \sim 50\,200\ cm^{-1} \quad (1)$$

where $R_e(TiF^+)$ is the equilibrium internuclear distance of TiF^+ (a typical value of ~ 1.75 Å was considered, see Ref. [5]), IP(TiII) = 13.63 eV [18] is the second ionisation potential of titanium, and EA(F) = 3.399 eV [19] is the electron affinity of fluorine. The stabilisation energy so obtained is sufficiently high that we may focus our attention on the $Ti^{2+}F^-$ ionic structure.

The ligand field model describing the Ti^{2+}–X^- structure was extensively presented previously [8] and only the main features will be reminded here. In this LFT model, the TiF^+ molecular energy levels are found by taking into account the splitting of the Ti^{2+} atomic levels due to the perturbation created by the F^- anion, considered as a point charge located at $R_e(TiF^+)$. We have considered in our calculations the two lowest-lying atomic configurations of Ti^{2+}: $3d^2$ (^3F, ^3P, ^1G, ^1D, ^1S) and $3d(^2D)4s$, which are expected to give rise to most of the low-lying electronic states of TiF^+. The calculations were carried out in Hund's case (a). The two configurations were treated simultaneously in a global matrix (the matrix elements are available from the authors upon request), including the d ~ s interaction between them. The importance of taking into account this interaction for a correct positioning of the electronic states was proved in the case of $TiCl^+$ [4,8]. The ligand field hamiltonian was defined by 12 parameters: $\Delta B_0^0(3d^2,3d4s) = B_0^0(3d^2) - B_0^0(3d4s)$, $B_0^2(3d^2)$, $B_0^2(3d4s)$, $B_0^4(3d^2)$, $B_0^4(3d4s)$, $B_0^2(3d^2,3d4s)$, $\zeta(3d^2)$, $\zeta(3d4s)$, $D(3d4s, 3d^2)$, $B(3d^2)$, $C(3d^2)$, and $G_2(3d,4s)$ (see, for example, Ref. [20] for a definition of the first six radial parameters B_0^k, and Ref. [21] for a definition of the last six atomic parameters). The atomic parameters, used to generate the electronic energy levels of Ti^{2+}, were held fixed in the fit at the following values, deduced from the Ti^{2+} free ion data of Ref. [22]: $\zeta(3d^2) = 121$ cm^{-1}, $\zeta(3d4s) = 114$ cm^{-1}, $D(3d4s,3d^2) = 32\,363$ cm^{-1}, $B(3d^2) = 835$ cm^{-1}, $C(3d^2) = 2924$ cm^{-1}, and $G_2(3d,4s) = 1689$ cm^{-1}. The radial parameters B_0^k for TiF^+ were calculated from the $TiCl^+$ corresponding values [8], taking into account their dependence on the internuclear separation $R_e(TiF^+)$. The following values were obtained: $\Delta B_0^0(3d^2,3d4s) \cong 25\,400$ cm^{-1}, $B_0^2(3d^2) \cong 16\,910$ cm^{-1}, $B_0^2(3d4s) \cong 17\,829$ cm^{-1}, $B_0^4(3d^2) \cong 6265$ cm^{-1}, $B_0^4(3d4s) \cong 7909$ cm^{-1}, and $B_0^2(3d^2,3d4s) \cong 15\,418$ cm^{-1}. Only three radial parameters, namely $\Delta B_0^0(3d^2,3d4s)$, $B_0^2(3d^2)$, and $B_0^2(3d^2,3d4s)$, were freely varied to fit the energy levels of the experimentally observed

$X^3\Phi$, $B^3\Delta$, $C^3\Pi$, and $[17.6]^3\Delta$ states of TiF^+. The fitted values of these parameters ($\Delta B_0^0(3d^2,3d4s) = 21\,012(36)$ cm^{-1}, $B_0^2(3d^2) = 14\,780(105)$ cm^{-1}, and $B_0^2(3d^2,3d4s) = 13\,798(40)$ cm^{-1}) are reasonably close to the initial calculated values mentioned above.

The excitation energies and the fractional characters resulting from the fit procedure are presented in Table 3. In the first column of this table are displayed (in parentheses) the dominant character of the calculated energy level, i.e. the basis function in-

Table 3
Excitation energies (in cm^{-1}) and fractional characters of the electronic states of TiF^+ arising from the $3d^2(^3F, ^3P, ^1G, ^1D, ^1S)$ and $3d(^2D)4s$ configurations of Ti^{2+}

No.[a]	Ω	Config.	Calc.	Exp.[b]	Composition[c]
1 ($^1\Sigma_{0_e}^+$)	0_e	$3d^2(^1G)$	63 301		0.96[1] + 0.04[4]
2 ($^1\Sigma_{0_e}^+$)	0_e	$3d^2(^1S)$	45 215		0.85[2] + 0.09[4] + 0.06[27]
3 ($^1\Pi_1$)	1	$3d^2(^1G)$	30 872		0.52[3] + 0.44[12] + 0.04[26]
4 ($^1\Sigma_{0_e}^+$)	0_e	$3d(^2D)4s$	28 135		0.85[4] + 0.11[2] + 0.03[1] + 0.01[27]
5 ($^3\Sigma_{0_f}^+$)	0_f	$3d(^2D)4s$	26 901		0.98[5] + 0.01[10] + 0.01[21]
6 ($^3\Sigma_1^+$)	1	$3d(^2D)4s$	26 895		0.98[6] + 0.01[8]
7 ($^3\Pi_2$)	2	$3d(^2D)4s$	26 262		0.52[7] + 0.40[18] + 0.07[28]
8 ($^3\Pi_1$)	1	$3d(^2D)4s$	26 191		0.52[8] + 0.40[19] + 0.07[29] + 0.01[6]
9 ($^3\Pi_{0_e}$)	0_e	$3d(^2D)4s$	26 137		0.52[9] + 0.40[20] + 0.07[31] + 0.01[4]
10 ($^3\Pi_{0_f}$)	0_f	$3d(^2D)4s$	26 126		0.52[10] + 0.40[21] + 0.07[32] + 0.01[5]
11 ($^1\Delta_2$)	2	$3d(^2D)4s$	24 836		0.48[11] + 0.40[13] + 0.10[25]
12 ($^1\Pi_1$)	1	$3d(^2D)4s$	18 599		0.55[12] + 0.44[3] + 0.01[26]
13 ($^1\Delta_2$)	2	$3d^2(^1G)$	18 359		0.45[13] + 0.36[25] + 0.18[11] + 0.01[15]
14 ($^3\Delta_3$)	3	$3d(^2D)4s$	17 963	17 971	0.81[14] + 0.19[30]
15 ($^3\Delta_2$)	2	$3d(^2D)4s$	17 842	17 843	0.79[15] + 0.19[33]
16 ($^3\Delta_1$)	1	$3d(^2D)4s$	17 730	17 721	0.81[16] + 0.19[34]
17 ($^1\Phi_3$)	3	$3d^2(^1G)$	16 053		1.00[17]
18 ($^3\Pi_2$)	2	$3d^2(^3P)$	14 924		0.53[18] + 0.45[7] + 0.01[28]
19 ($^3\Pi_1$)	1	$3d^2(^3P)$	14 863		0.53[19] + 0.45[8] + 0.01[29]
20 ($^3\Pi_{0_e}$)	0_e	$3d^2(^3P)$	14 803		0.53[20] + 0.45[9] + 0.01[31]
21 ($^3\Pi_{0_f}$)	0_f	$3d^2(^3P)$	14 802		0.53[21] + 0.45[10] + 0.01[32]
22 ($^3\Sigma_1^-$)	1	$3d^2(^3P)$	11 590		0.81[22] + 0.17[35] + 0.02[26]
23 ($^3\Sigma_{0_e}^-$)	0_e	$3d^2(^3P)$	11 578		0.83[23] + 0.17[36]
24 ($^1\Gamma_4$)	4	$3d^2(^1G)$	11 211		1.00[24]
25 ($^1\Delta_2$)	2	$3d^2(^1D)$	11 198		0.53[25] + 0.40[11] + 0.06[13]
26 ($^1\Pi_1$)	1	$3d^2(^1D)$	10 667		0.92[26] + 0.04[3] + 0.02[22] + 0.01[12]
27 ($^1\Sigma_{0_e}^+$)	0_e	$3d^2(^1D)$	10 123		0.92[27] + 0.04[4] + 0.04[2]
28 ($^3\Pi_2$)	2	$3d^2(^3F)$	2473		0.71[28] + 0.18[33] + 0.05[15] + 0.05[18] + 0.01[7]
29 ($^3\Pi_1$)	1	$3d^2(^3F)$	2413	2382	0.76[29] + 0.13[34] + 0.05[19] + 0.03[16] + 0.02[8] + 0.01[35]
30 ($^3\Delta_3$)	3	$3d^2(^3F)$	2374		0.81[30] + 0.19[14]
31 ($^3\Pi_{0_e}$)	0_e	$3d^2(^3F)$	2321	2319	0.88[31] + 0.06[20] + 0.03[36] + 0.02[9] + 0.01[23]
32 ($^3\Pi_{0_f}$)	0_f	$3d^2(^3F)$	2285	2319	0.92[32] + 0.06[21] + 0.02[10]
33 ($^3\Delta_2$)	2	$3d^2(^3F)$	2187	2219	0.62[33] + 0.21[28] + 0.14[15] + 0.01[18]
34 ($^3\Delta_1$)	1	$3d^2(^3F)$	2078	2115	0.67[34] + 0.16[16] + 0.14[29] + 0.01[19]
35 ($^3\Sigma_1^-$)	1	$3d^2(^3F)$	1305		0.81[35] + 0.17[22] + 0.02[29]
36 ($^3\Sigma_{0_e}^-$)	0_e	$3d^2(^3F)$	1282		0.79[36] + 0.17[23] + 0.03[31]
37 ($^3\Phi_4$)	4	$3d^2(^3F)$	368	360	1.00[37]
38 ($^3\Phi_3$)	3	$3d^2(^3F)$	181	180	1.00[38]
39 ($^3\Phi_2$)	2	$3d^2(^3F)$	0	0	1.00[39]

[a] The label in parentheses represents the basis function involved at the highest extent in the expansion listed in the last column, i.e. the dominant character of the level.

[b] The relative positions of the spin-orbit components are based on the assumption that $A(X^3\Phi) = 60$ cm^{-1} (see text).

[c] The numbers in square brackets refer to the corresponding numbers in the first column, i.e. to the basis functions designed by these numbers.

volved at the highest extent in the expansion listed in the last column. The numbers in square brackets in the last column refer to the corresponding numbers in the first column, i.e. to the basis function designed by these numbers. As one can observe, strong mixing of basis functions occurs for some of the levels listed in Table 3 and, strictly speaking, these states belong to the Hund's case (c), i.e. Ω is the only good quantum number for them. For this reason, we have listed in the second column of Table 3 the corresponding Ω for every calculated level, as the only strict level's label. As already noted in Section 4, we must emphasise that the spin-orbit intervals between different Ω levels of a given electronic state were not determined for TiF^+ and the 'experimental' excitation energies displayed in the fourth column of Table 3 are based on the assumption $A(X^3\Phi) \cong \zeta(3d^2)/2 \cong 60\ cm^{-1}$ (see Ref. [23] for a proof of the first equation).

Overall, we can observe that our model is able to reproduce the experimental spectrum of TiF^+ with reasonable accuracy. The slight remaining differences (a few tens of cm^{-1} at most) between experimental and calculated positions of the energy levels can be attributed to several reasons, like the assumption mentioned above, the choice of a unique value of R_e for all the states (parallel potential energy curves), or the choice of a unique (and fixed) value of spin-orbit parameters for all the states arising from the same electronic configuration. The new predictions so obtained could help future identifications of electronic states of TiF^+: it would be interesting, for instance, to observe the $C^3\Pi - A^3\Sigma^-$ allowed transition in the IR, which should be situated, according to our calculations, in a spectral region ($\sim$1000–1100 cm^{-1}) fully accessible to the diode lasers and expecting the $A^3\Sigma^-$ state to be populated enough to make absorption experiments possible. The identification of the $A^3\Sigma^-$ electronic state would so complete the picture of the low-lying electronic states of TiF^+. Regarding this low excitation energy region, an interesting comparison can be made between the two isovalent species $TiCl^+$ and TiF^+. So, while the $3d^2[^3F]$ monoconfigurational LFT calculations should give rise to the $^3\Phi < ^3\Sigma^- < ^3\Pi < ^3\Delta$ energy ordering (as obtained by Kaledin et al. [9] for $TiCl^+$), the d $\sim$ s interaction between the $3d^2$ and 3d4s configurations is very strong in the case of $TiCl^+$ and leads to the $^3\Phi < ^3\Delta < ^3\Sigma^- < ^3\Pi$ energy ordering, with an important downward shift for the $^3\Delta$ ($3d^2$) state (see Table 5 of Ref. [8]). In contrast, in the case of TiF^+ the global effect of this interaction turns out to be less important, leading to a $^3\Phi < ^3\Sigma^- < ^3\Delta < ^3\Pi$ energy ordering (see Table 3). At a first sight this can seem surprising, as the d $\sim$ s interaction parameter $B_0^2(3d^2,3d4s)$ was found to be larger for TiF^+ ($13\,798 \pm 40\ cm^{-1}$) than for $TiCl^+$ ($12\,535 \pm 5\ cm^{-1}$, see Table 5 of Ref. [8]) and the relative positions of the $^3\Delta$ (3d4s) and $^3\Delta$ ($3d^2$) states are approximately the same. Fractional characters for these states further indicate that the d $\sim$ s interaction has about the same strength in TiF^+ and $TiCl^+$. However, one should note that the $B_0^2(3d^2)$ and $B_0^4(3d^2)$ parameters control the relative positions of the $^3\Phi$ ($3d^2$), $^3\Delta$ ($3d^2$), $^3\Pi$ ($3d^2$) and $^3\Sigma^-$ ($3d^2$) states in addition to the $B_0^2(3d^2,3d4s)$ parameter, and the values of these parameters are significantly different in TiF^+ when compared to those of $TiCl^+$, due to an important difference in the equilibrium distances ($R_e(TiCl^+) \cong 2.18$ Å [2], $R_e(TiF^+) \cong 1.75$ Å [5]). Consequently, even if the downward shift of the $^3\Delta$ ($3d^2$) state due to the d $\sim$ s interaction is larger for TiF^+ than for the isovalent $TiCl^+$, this is not strong enough to push the $^3\Delta$ ($3d^2$) state below the $^3\Sigma^-$ ($3d^2$) state. In this respect, the d $\sim$ s interaction exhibits globally less important effects in TiF^+ than in $TiCl^+$.

Considering the higher excitation energy of the $^3\Delta$ ($3d^2$) state in TiF^+ compared to $TiCl^+$, we are able now to explain the absence of 'satellite' ($\Delta\Sigma \neq 0$) bands in the experimental spectrum of the $[17.6]^3\Delta - X^3\Phi$ transition of TiF^+ [5], which prevented the experimental determination of the spin-orbit constants for this species. While in the case of $TiCl^+$ it was the close-lying positions of the $X^3\Phi$ and $A^3\Delta$ states that led to the observation of these 'satellite' bands and of strong perturbations between the two electronic states, for TiF^+ the $X^3\Phi$ is far from the potentially perturbing $B^3\Delta$ state and their interaction is not strong enough to generate visible perturbations on the experimental spectrum. However, we may note that the $B^3\Delta$ state of TiF^+ is very close to the $C^3\Pi$ state and one can expect that strong perturbations occur between these two states. It would be very interesting to explore this spectral region at high resolution in order to evidence such peculiar

details, which cannot be observed using low-resolution techniques.

6. Discussion and conclusion

The results displayed in this paper are of interest for two reasons. First some enlightenment has been pointed out about the electronic structure of $TiCl^+$ and TiF^+. Despite the low resolution it is now possible to locate the expected transitions on the basis of experimental matter rather than on theoretical information which is less accurate. For example one can predict that the origin of the $C^3\Pi_0 - A^3\Delta_1$ transition of $TiCl^+$ is close to 1254 cm^{-1}, in the same way the $B^3\Delta - X^3\Phi$ transition of TiF^+ can be also easily located. This information is of interest for further laser experiments in the infrared, mainly on a time-saving point of view. The weakness of the fluorescence signal does not encourage to record high dispersed spectra in the visible, but it could be of interest to test if in the infrared spectral region the $C^3\Pi - A^3\Delta$ transition of $TiCl^+$ and the $B^3\Delta - X^3\Phi$ transition of TiF^+ could not be observed when the upper states are indirectly populated via the $[17.8]^3\Delta$ state of $TiCl^+$ or the $[17.6]^3\Delta$ state of TiF^+. New interest in the spectra of $TiCl^+$ and TiF^+ could be found on the basis of this work.

On the other hand, we demonstrate in this paper that it is possible to observe fluorescence signal of diatomic ions despite the low concentration of the ions produced in the discharge. High resolution laser excitation spectroscopy is of less interest when compared to the velocity modulation laser technique which is quite independent from the noisy emission of the source and eliminates signal from neutral molecules. Nevertheless, in some cases, blended bands could be individually recorded as routinely done for neutral molecules when spectra of overlapped bands induce fluorescence signals which can be collected in different spectral regions through a spectrometer used as a narrow-band filter [24]. Experiments such as saturation spectroscopy could also be attempted in order to analyze the hyperfine structure.

Dispersed laser-induced fluorescence experiments cannot be considered as sufficient to understand the electronic structure of a molecule but rather as an auxiliary technique to further high resolution analyses of electronic transitions. On the other hand, without the frame given by the previous works done on $TiCl^+$ and TiF^+ which limits the hypotheses and secures the interpretation, it is obvious that misinterpretations could have been carried out. This is especially the case for transition-elements compounds because these molecules are characterised by numerous low-lying electronic states separated by intervals the values of which are often similar to their vibrational constants.

The work done in our laboratory on $TiCl^+$ and TiF^+ lies on three complementary approaches which contributed to the building-up of the electronic structure of the low-lying states of these two ions. First: high resolution spectroscopy leading to accurate determination of some electronic states. Second: low-resolution dispersed fluorescence experiments, attempted here for the first time on metallic diatomic ions, which give access to the identification of new electronic states, out of reach from absorption techniques, at least in the visible spectral range. Third: theoretical approach which provides the frame of these studies but also takes advantage of experimental data.

We expect that new enlightenment collected all along this work will encourage new high resolution experiments to be performed, especially in the infrared spectral region.

Acknowledgements

We thank one of the referees for pointing out some particular aspects in the LFT treatment. David Collet and Dr. Thérèse R. Huet are thanked for their collaboration during this work. The Centre d'Etudes et de Recherches Lasers et Applications is supported by the Ministère Chargé de la Recherche, the région Nord–Pas de Calais, and the Fonds Européen de Développement Economique des Régions.

References

[1] C. Focsa, C. Dufour, B. Pinchemel, I. Hadj Bachir, T.H. Huet, J. Chem. Phys. 106 (1997) 9044.
[2] C. Focsa, B. Pinchemel, J.L. Féménias, T.H. Huet, J. Chem. Phys. 107 (1997) 10365.

[3] L.A. Kaledin, M.C. Heaven, J. Mol. Spectrosc. 184 (1997) 113.
[4] L.A. Kaledin, M.C. Heaven, J. Chem. Phys. 107 (1997) 7020.
[5] C. Focsa, B. Pinchemel, D. Collet, T.H. Huet, J. Mol. Spectrosc. 189 (1998) 254.
[6] C.S. Gudeman, C.C. Martner, R.J. Saykally, Phys. Rev. Lett. 50 (1983) 727.
[7] L.A. Kaledin, A.L. Kaledin, M.C. Heaven, J. Mol. Spectrosc. 179 (1996) 246.
[8] C. Focsa, M. Bencheikh, L.G.M. Pettersson, J. Phys. B: At. Mol. Opt. Phys. 31 (1998) 2857.
[9] L.A. Kaledin, J.E. McCord, M.C. Heaven, J. Mol. Spectrosc. 173 (1995) 499.
[10] W.J. Balfour, K.S. Chandrasekhar, J. Mol. Spectrosc. 139 (1990) 245.
[11] H.J. Andrä, A. Gaupp, W. Wittmann, Phys. Rev. Lett. 31 (1973) 501.
[12] L.S. Kaufman, Opt. Commun. 17 (1976) 309.
[13] S.D. Rosner, T.D. Gaily, R.A. Holt, Phys. Rev. A 26 (1982) 697.
[14] M. Larzillière, J. Lacoursière, M. Chafik el Idrissi, N. Varfalvy, P. Lafleur, A.J. Ross, Phys. Rev. A 48 (1993) 471.
[15] N. Varfalvy, P. Lafleur, M. Larzillière, J. Mol. Spectrosc. 177 (1996) 1.
[16] G. Herzberg, Spectra of Diatomic Molecules, 2nd edn., van Nostrand, Princeton, 1950.
[17] M.L. Mandich, M.L. Steigerwald, W.D. Reents Jr., J. Am. Chem. Soc. 108 (1986) 6197.
[18] C.E. Moore, Atomic Energy Levels, Vols. 1 and 2, National Bureau of Standards, 1952.
[19] H. Hotop, W.C. Lineberger, J. Phys. Chem. Ref. Data 4 (1975) 539.
[20] R.W. Field, Ber. Bunsenges. Phys. Chem. 86 (1982) 771.
[21] J.S. Griffith, The Theory of Transition-Metal Ions, Cambridge University Press, 1961.
[22] Y. Shami, E. Caspi, J. Oreg, J. Res. Nat. Bur. Stand. A 73 (1969) 173.
[23] H. Lefebvre-Brion, R.W. Field, Perturbations in the Spectra of Diatomic Molecules, Academic Press, New York, 1986.
[24] C. Focsa, C. Dufour, B. Pinchemel, J. Mol. Spectrosc. 182 (1997) 65.